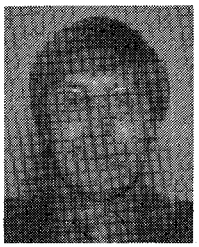

Anthony Dandridge was born in Kent, England, on November 11, 1951. He received the B.Sc. and Ph.D. degrees in physics from the Sir John Cass School of Science and Technology, City of London Polytechnic, England.

His postgraduate and postdoctoral research work included flow birefringence and light scattering studies of short chain polymers. In 1979 he was a Lecturer in Physics at the University of Kent, Canterbury, England. Since 1980 he has been associated with Georgetown University, Washington, DC, John Carroll University, Cleveland, OH, and the Naval Research Laboratory, Washington, DC. His research work covers fiber optic sensor systems and the noise and spectral characteristics of semiconductor lasers.

Dr. Dandridge is a Fellow of the Royal Astronomical Society.

Joseph F. Weller was born in Louisville, KY in 1939. He received the B.S. degree in physics from Xavier University, Cincinnati, OH, in 1960, and the M.S. and Ph.D. degrees in physics from American University, Washington, DC, in 1968 and 1972, respectively.

He joined the Naval Research Laboratory, Washington, DC, in 1960 where he began work on radiation damage on semiconductor devices. Since then he has been active in areas of quantum electronics and ultrasonics. His research interests have included rare earth spectroscopy in glasses, glass lasers, nonlinear optics, and optical interactions with surface acoustic waves. He is presently Head of the Optical Hybrid Devices Section of the Optical Techniques Branch. His current research interests include properties of laser diodes and optical interactions in microwave and millimeter wave devices.

Dr. Weller is a member of the American Physical Society.

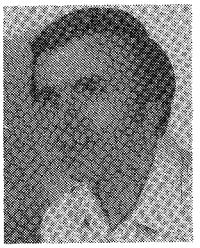

Ronald O. Miles (S'66–M'77) was born in Salt Lake City, UT, on November 25, 1940. He received the B.S. degree in electrical engineering in 1967, and the M.S. and Ph.D. degrees in 1973 and 1978, respectively, all from the University of Utah, Salt Lake City.

While at the University of Utah he was a Teaching Assistant and Research Assistant in the Microwave Device and Physical Electronics Laboratory, where his primary interest has been in CO_2 laser plasma diagnostics and CO_2 waveguide lasers. In 1974 he was a Consultant on preliminary design of a gas dynamic laser for a laser-driven ionization process for applications in MHD power-generating systems for the Department of Mechanical Engineering, University of Utah. From 1975 to 1976 he was a Consultant on laser applications in development of new processes for preventive denistry for the Department of Mechanical Engineering, University of Utah. His research interests include hollow-core distributed-feedback waveguide lasers. Since 1978 he has been with the Naval Research Laboratory, Washington, DC, where his research is on noise in semiconductor lasers and laser fiber sensor systems.

Dr. Miles is a member of the American Physical Society, the Optical Society of America, and Sigma Xi.

Noise in an AlGaAs Semiconductor Laser Amplifier

TAKAAKI MUKAI AND YOSHIHISA YAMAMOTO, MEMBER, IEEE

Abstract—**The noise characteristics in a Fabry-Perot (FP) cavity type semiconductor laser amplifier, biased at just below its oscillation threshold current, have been studied theoretically and experimentally. Quantum mechanical multimode rate equations containing a Langevin shot noise source and an input signal term were numerically solved for an exponential band-tail model with no *k*-selection rule. Noise power calculated using this rate equation was compared with a simpler photon statistic master equation method. The experimental results on noise power for an AlGaAs laser amplifier are in reasonable agreement with the two different theoretical predictions. Dominant noise powers in a semiconductor laser amplifier are beat noise powers between signal and spontaneous emission, and between spontaneous emission components. Noise characteristics in a Fabry-Perot cavity type laser amplifier can be improved both by the reduction of the facet mirror reflectivities and by use of an asymmetric cavity configuration with low-input and high-output mirror reflectivities. Two beat noise powers are expressed in simple analytic form by introducing an equivalent noise bandwidth and an excess noise coefficient as figures of merit in an optical amplifier.**

Manuscript received September 1, 1981; revised December 7, 1981.

The authors are with the Musashino Electrical Communication Laboratory, Nippon Telegraph and Telephone Public Corporation, Tokyo, Japan.

I. INTRODUCTION

APPLICATIONS of semiconductor laser amplifiers have been studied, both to a PCM-IM direct detection optical transmission system [1], and a coherent optical fiber transmission system [2]. Experimental results with signal gain [3], [4], link gain [5], frequency bandwidth [4], saturation output power [4], and preamplifier performance for a 100 Mbit/s PCM-IM signal [6], [7] of a Fabry-Perot (FP) cavity type AlGaAs laser amplifier have been reported. These works indicate that an FP cavity type semiconductor laser amplifier is promising as an optical linear repeater in these systems.

The noise characteristics of a semiconductor laser amplifier are indispensable in estimating the S/N performance of optical direct amplification transmission systems. Amplitude noise in semiconductor lasers was originally measured by Armstrong and Smith, using a Hanbury Brawn-Twiss experiment [8]. Paoli *et al.* measured the resonance peak of AM noise [9]. Recently, Jäckel *et al.* measured the quantum-noise-limited intensity fluctuation in a transverse-mode-stabilized CSP laser [10], and reported that the noise behavior of a CSP laser agrees

0018-9480/82/0400-0410$00.75

reasonably with that predicted by McCumber's theory.

Noise characteristics in a semiconductor laser amplifier, however, seem to be quite different from those in a semiconductor laser oscillator because the amplifier operates at just below its oscillation threshold current, where noisy multilongitudinal amplified spontaneous emission contributes to total noise power. An additional reason for this difference is that the noise induced by the external input signal light seems to play an important role [11].

In this paper, noise power and its spectrum dependences on dc bias current, amplified signal level, and signal gain are studied theoretically and experimentally for an FP cavity type AlGaAs double-heterostructure (DH) laser amplifier. Quantum mechanical multimode rate equations containing a Langevin shot noise source, originally derived by McCumber [12], are extended here to involve an input signal term. They are based on a band-tail model, with no k-selection rule, for a GaAs laser [13]. The results are compared with that by a simpler photon statistic master equation analysis [14]. They are also compared with experimental results. Noise characteristics are calculated to depend on facet mirror reflectivity. Two beat noise powers are expressed in simple analytic form by introducing an equivalent noise bandwidth and an excess noise coefficient, which are the figures of merit of an FP cavity type laser amplifier.

II. Theoretical Formulation

A. Rate Equation Analysis

Multimode rate equations with McCumber's fluctuation operator [12], [15] have been extended to involve an input signal term, so that

$$\frac{dN_e}{dt} = P - R_{sp}^T - \sum_m G_m \Gamma N_{p,m} + F_e(t), \tag{1}$$

$$\frac{dN_{p,m}}{dt} = -\frac{N_{p,m}}{\tau_p} + G_m \Gamma N_{p,m} + E_{cv,m}\Gamma + P_{in,m} + F_{p,m}(t). \tag{2}$$

Here, N_e is the total number of carriers in the active region, $N_{p,m}$ is the total number of photons in the mth longitudinal mode, P is the pumping rate, R_{sp}^T is the spontaneous emission probability coupled to both guided and all unguided modes, and that is conventionally expressed by N_e/τ_s, τ_s is the carrier lifetime, $E_{cv,m}$ is the spontaneous emission probability coupled to the mth longitudinal guided mode, G_m is the stimulated emission coefficient of the mth longitudinal guided mode and is derived as $E_{cv,m} - E_{vc,m}$, $E_{vc,m}$ is the stimulated absorption probability of the mth longitudinal guided mode, $P_{in,m}$ is the number of signal photons injected into the mth longitudinal guided mode, Γ is the factor of mode confinement to the active region, τ_p is the photon lifetime, and $F_e(t)$ and $F_{p,m}(t)$ are, respectively, the fluctuation operators [15] for the number of carriers and the number of photons in the mth longitudinal mode.

An exponential band-tail model with no k-selection rule [13] is used here to describe the band structure of AlGaAs semiconductor lasers operating at room temperature. In this model, the parameters R_{sp}^T, G_m, and $E_{cv,m}$ are expressed analytically as a function of carrier number N_e as follows [16]:

$$R_{sp}^T = \frac{N_e}{\tau_s} = \frac{B}{\eta_L V} \cdot N_e(N_e + N_A^- - N_D^+) \tag{3}$$

where B is the recombination coefficient, V is the volume of the active region, η_L is laser internal quantum efficiency, and N_A^- and N_D^+ are the total number of ionized acceptors and donors, respectively.

The stimulated emission coefficient G_0 for the gain central longitudinal mode is

$$G_0 = C_1 \cdot N_e(N_e + N_A^- - N_D^+) \tag{4}$$

$$C_1 = \frac{B}{E_0 V^2 \phi \exp(1)} \cdot \left[\frac{\sin(kT\pi/E_0)}{kT\pi/E_0}\right]^2 \tag{5}$$

where E_0 is the band-tailing parameter, and $\Phi = 8\pi n^3 E^2/h^3 c^3$ is the spatial mode number per unit volume and energy.

The stimulated emission coefficient G_m for other longitudinal modes is approximated by

$$G_m = G_0 \left[1 - \left(\frac{m\Delta E_m}{\Delta E}\right)^2\right] \tag{6}$$

where ΔE_m is the energy separation corresponding to the longitudinal mode spacing.

The spontaneous emission probability $E_{cv,m}$ is given by

$$E_{cv,m} = \frac{G_m}{1 - \exp(-E_0/kT)}. \tag{7}$$

McCumber [12] has indicated that intrinsic quantum fluctuation can be incorporated into the rate equations by introducing the fluctuation operators $F_e(t)$ and $F_{p,m}(t)$, whose correlation functions and noise spectra correspond to those derived by photon statistic master equation analysis [14]. The intrinsic fluctuation stems from the shot noise-like fluctuations in the particle flow rates in the laser because the carrier and photon population operators are variables with integral values.

Carrier and photon number fluctuation operators $F_e(t)$ and $F_{p,m}(t)$ as Langevin noise sources are assumed to have shot noise character in the following manner [12], [15], [17]:

$$\langle F_e(t)\rangle = \langle F_{p,m}(t)\rangle = 0, \tag{8}$$

$$\langle F_e(t) \cdot F_e(s)\rangle = \delta(t-s) \cdot \left\{P + R_{sp}^T + \sum_m [E_{cv,m}\Gamma N_{p,m} + (E_{cv,m} - G_m)\Gamma N_{p,m}]\right\}, \tag{9}$$

$$\langle F_{p,m}(t) \cdot F_{p,m}(s)\rangle = \delta(t-s) \cdot \left[\frac{N_{p,m}}{\tau_p} + E_{cv,m}\Gamma(1 + N_{p,m}) + (E_{cv,m} - G_m)\Gamma N_{p,m} + P_{in,m}\right], \tag{10}$$

$$\langle F_e(t) \cdot F_{p,m}(s)\rangle = \langle F_{p,m}(t) \cdot F_e(s)\rangle = -\delta(t-s) \cdot [E_{cv,m}\Gamma(1 + N_{p,m}) + (E_{cv,m} - G_m)\Gamma N_{p,m}]. \tag{11}$$

The average value of the fluctuation vanishes by (8), which implies that stationary characteristics, such as signal gain, can be analyzed using (1) and (2) without fluctuation operators. The delta function $\delta(t-s)$ describes the shot noise character.

The correlation of the carrier number fluctuation in (9) is

induced by the pumping, the spontaneous emission coupled to both guided and radiation modes, the stimulated emission, and the stimulated absorption. The correlation of the photon number fluctuation in (10) is induced by the photon escape from the cavity, the spontaneous emission, the stimulated emission, the stimulated absorption, and the signal photon input to the mth longitudinal mode. The cross-correlation fluctuation between carrier and photon number in (11) is induced by the spontaneous emission, the stimulated emission, and the stimulated absorption.

The numbers of carriers and photons are expressed by fluctuations around the mean values, in the form

$$N_e = \bar{N}_e + \Delta N_e$$
$$N_{p,m} = \bar{N}_{p,m} + \Delta N_{p,m}. \tag{12}$$

Expanding the transition rates to the first order in ΔN_e, we obtain

$$R_{sp}^T = \bar{R}_{sp}^T + \frac{\partial \bar{R}_{sp}^T}{\partial \bar{N}_e} \cdot \Delta N_e,$$
$$E_{cv,m} = \bar{E}_{cv,m} + \frac{\partial \bar{E}_{cv,m}}{\partial \bar{N}_e} \cdot \Delta N_e,$$
$$G_m = \bar{G}_m + \frac{\partial \bar{G}_m}{\partial \bar{N}_e} \cdot \Delta N_e. \tag{13}$$

Using (12) and (13) in (1) and (2), and neglecting the products of small quantities, we obtain the following linearized equations for the fluctuations:

$$\frac{d}{dt}\Delta N_e(t) = \left(-\frac{\partial \bar{R}_{sp}^T}{\partial \bar{N}_e} - \sum_m \frac{\partial \bar{G}_m}{\partial \bar{N}_e} \cdot \Gamma \bar{N}_{p,m}\right) \cdot \Delta N_e(t) - \sum_m \bar{G}_m \Gamma \cdot \Delta N_{p,m}(t) + F_e(t), \tag{14}$$

$$\frac{d}{dt}\Delta N_{p,m}(t) = \Gamma\left(\bar{N}_{p,m}\frac{\partial \bar{G}_m}{\partial \bar{N}_e} + \frac{\partial \bar{E}_{cv,m}}{\partial \bar{N}_e}\right) \cdot \Delta N_e(t) + \left(\bar{G}_m \Gamma - \frac{1}{\tau_p}\right) \cdot \Delta N_{p,m}(t) + F_{p,m}(t). \tag{15}$$

Equation (14) indicates that the time variation of the carrier number fluctuation is influenced by both the carrier fluctuation through the total spontaneous and stimulated emissions, the photon fluctuation through the total stimulated emission, and the intrinsic quantum carrier fluctuation source. The contribution of the carrier fluctuation stems from the perturbation in both the spontaneous emission probability and the stimulated emission coefficient. Equation (15) indicates that the time variation of the photon number fluctuation of the mth longitudinal mode is influenced by both the carrier fluctuation through the spontaneous and stimulated emissions to the mth longitudinal mode, the photon fluctuation of the mth longitudinal mode through both the stimulated emission and the photon escape from the cavity, and the intrinsic quantum photon fluctuation source.

The Fourier transforms of (14) and (15) are

$$j\omega \cdot \Delta N_e(\omega) = A_1 \cdot \Delta N_e(\omega) + \sum_m A_{2,m} \cdot \Delta N_{p,m}(\omega) + F_e(\omega) \tag{16}$$

$$j\omega \cdot \Delta N_{p,m}(\omega) = A_{3,m} \cdot \Delta N_e(\omega) + A_{4,m} \cdot \Delta N_{p,m}(\omega) + F_{p,m}(\omega) \tag{17}$$

where

$$A_1 = -\frac{\partial \bar{R}_{sp}^T}{\partial \bar{N}_e} - \sum_m \frac{\partial \bar{G}_m}{\partial \bar{N}_e} \cdot \Gamma \bar{N}_{p,m},$$
$$A_{2,m} = -\bar{G}_m \Gamma,$$
$$A_{3,m} = \Gamma\left(\bar{N}_{p,m}\frac{\partial \bar{G}_m}{\partial \bar{N}_e} + \frac{\partial \bar{E}_{cv,m}}{\partial \bar{N}_e}\right),$$
$$A_{4,m} = \bar{G}_m \Gamma - \frac{1}{\tau_p}. \tag{18}$$

In (16) and (17) $\Delta N_e(\omega)$, $\Delta N_{p,m}(\omega)$, $F_e(\omega)$, and $F_{p,m}(\omega)$ can be defined as

$$\Delta N_e(t) = \int_{-\infty}^{+\infty} \Delta N_e(\omega)\, e^{j\omega t}\, d\omega,$$
$$\Delta N_{p,m}(t) = \int_{-\infty}^{+\infty} \Delta N_{p,m}(\omega)\, e^{j\omega t}\, d\omega,$$
$$F_e(t) = \int_{-\infty}^{+\infty} F_e(\omega)\, e^{j\omega t}\, d\omega,$$
$$F_{p,m}(t) = \int_{-\infty}^{+\infty} F_{p,m}(\omega)\, e^{j\omega t}\, d\omega. \tag{19}$$

The Fourier component $\Delta N_{p,m}(\omega)$ of the photon number fluctuation in the mth longitudinal mode is obtained from (16) and (17) as

$$\Delta N_{p,m}(\omega) = \frac{F_{p,m}(\omega)}{j\omega - A_{4,m}} + \frac{A_{3,m}}{j\omega - A_{4,m}} \cdot \frac{F_e(\omega) + \sum_m \dfrac{A_{2,m} F_{p,m}(\omega)}{j\omega - A_{4,m}}}{\alpha} \tag{20}$$

where

$$\alpha \equiv \alpha_R + j\alpha_I = -A_1 + \sum_m \frac{A_{2,m}A_{3,m}A_{4,m}}{\omega^2 + A_{4,m}^2} + j\omega\left[1 + \sum_m \frac{A_{2,m}A_{3,m}}{\omega^2 + A_{4,m}^2}\right]. \tag{21}$$

Equation (20) indicates that the Fourier component of the photon number fluctuation in the mth longitudinal mode is caused by the intrinsic quantum fluctuation sources $F_e(\omega)$ and $F_{p,m}(\omega)$ through the following processes listed just below.

The first process is the direct contribution of the intrinsic photon fluctuation source $F_{p,m}$ in the mth longitudinal mode, as expressed by the first term on the right-hand side of (20). The photon fluctuation source $F_{p,m}$ is multiplied by $1/(j\omega + 1/\tau_p - \bar{G}_m\Gamma)$, which indicates the existence of a resonance-free spectrum with low-pass filter characteristics. The amplification factor in the low-frequency region is determined by the reciprocal value of the difference between the theoretical threshold gain and the actual gain.

The second process is that expressed by the second term on

the right-hand side of (20), in which the intrinsic carrier fluctuation source F_e contributes to the photon fluctuation in the mth longitudinal mode through the spontaneous and stimulated emissions. The term F_e is multiplied by $1/\alpha$, which represents the effect of interaction between photons and carriers, and indicates the resonance peak spectrum above the threshold current.

The third process is expressed by the third term on the right-hand side of (20), in which the total intrinsic photon fluctuation sources $\Sigma_m F_{p,m}$ contribute to the carrier fluctuation through the stimulated emission. Furthermore, the induced carrier fluctuation contributes to the photon fluctuation in the mth longitudinal mode through the spontaneous and stimulated emissions.

The self-correlation spectrum for the photon number fluctuation in the mth longitudinal mode is given by [18]

$$\begin{aligned}\langle \Delta N_{p,m}(\omega)\cdot \Delta N^*_{p,m}(\omega)\rangle &= \frac{1}{\omega^2+A_{4,m}^2}\cdot\left\{\frac{A_{3,m}^2}{\alpha\cdot\alpha^*}\cdot\langle F_e^2(\omega)\rangle\right.\\ &+\left[1+\frac{A_{3,m}^2}{\alpha\cdot\alpha^*}\cdot\sum_m\frac{A_{2,m}^2}{\omega^2+A_{4,m}^2}\right.\\ &\left.+\frac{2A_{2,m}A_{3,m}(-\alpha_R A_{4,m}-\omega\alpha_I)}{\alpha\cdot\alpha^*(\omega^2+A_{4,m}^2)}\right]\cdot\langle F_{p,m}^2(\omega)\rangle\\ &+\left[\frac{-A_{3,m}^2}{\alpha\cdot\alpha^*}\cdot\sum_m\frac{2A_{2,m}A_{4,m}}{\omega^2+A_{4,m}^2}+\frac{2\alpha_R A_{3,m}}{\alpha\cdot\alpha^*}\right]\\ &\left.\cdot\langle F_e(\omega)\cdot F_{p,m}(\omega)\rangle\right\} \qquad (22)\end{aligned}$$

where α^* denotes the complex conjugate of α in (21).

The cross-correlation spectrum for the photon number fluctuation between the kth and lth longitudinal modes given by

$$\begin{aligned}\langle \Delta N_{p,k}(\omega)\cdot \Delta N^*_{p,l}(\omega)\rangle &= \frac{1}{(j\omega-A_{4,k})(-j\omega-A_{4,l})}\cdot\left\{\frac{A_{3,k}A_{3,l}}{\alpha\cdot\alpha^*}\right.\\ &\cdot\left[\langle F_e^2(\omega)\rangle-\sum_m\frac{2A_{4,m}A_{2,m}}{\omega^2+A_{4,m}^2}\cdot\langle F_e(\omega)\cdot F_{p,m}(\omega)\rangle\right.\\ &\left.+\sum_m\frac{A_{2,m}^2}{\omega^2+A_{4,m}^2}\cdot\langle F_{p,m}^2(\omega)\rangle\right]\\ &+\frac{A_{3,l}A_{2,k}}{\alpha^*(-j\omega-A_{4,k})}\cdot\langle F_{p,k}^2(\omega)\rangle\\ &+\frac{A_{3,k}A_{2,l}}{\alpha(j\omega-A_{4,l})}\cdot\langle F_{p,l}^2(\omega)\rangle+\frac{A_{3,l}}{\alpha^*}\cdot\langle F_e(\omega)\\ &\left.\cdot F_{p,k}(\omega)\rangle+\frac{A_{3,k}}{\alpha}\cdot\langle F_e(\omega)\cdot F_{p,l}(\omega)\rangle\right\}. \qquad (23)\end{aligned}$$

The self-correlation spectrum (22) denotes the photon number fluctuation in the mth longitudinal mode itself. On the other hand, the cross-correlation spectrum (23) denotes the photon number fluctuation originating in the interaction between the kth and lth longitudinal modes. The sign of the cross-correlation spectrum is plus or minus, depending on both the dc bias current and the number of photons in the related longitudinal modes. The noise power obtained by the summation of the self-correlation spectrum alone, over the total of the longitudinal modes, attains a value greater than that calculated by about 15 dB, including both self- and cross-correlation spectra. This indicates that the total noise power is reduced by the interaction between different longitudinal modes. This phenomenon has been observed in a multimode oscillating AlGaAs laser [19], [20].

The mean-squared fluctuation density of the intrinsic quantum noise source is given by the Fourier transformation of correlation functions (9)-(11) as

$$\begin{aligned}\langle F_e^2(\omega)\rangle &= P+\bar{R}_{sp}^T+\sum_m\left[\bar{E}_{cv,m}\Gamma\bar{N}_{p,m}\right.\\ &\left.+(\bar{E}_{cv,m}-\bar{G}_m)\Gamma\bar{N}_{p,m}\right], \qquad (24)\\ \langle F_{p,m}^2(\omega)\rangle &= \frac{\bar{N}_{p,m}}{\tau_p}+\bar{E}_{cv,m}\bar{\Gamma}(1+\bar{N}_{p,m})\\ &+(\bar{E}_{cv,m}-\bar{G}_m)\Gamma\bar{N}_{p,m}+P_{in,m}, \qquad (25)\\ \langle F_e(\omega)\cdot F_{p,m}(\omega)\rangle &= -\bar{E}_{cv,m}\Gamma(1+\bar{N}_{p,m})\\ &-(\bar{E}_{cv,m}-\bar{G}_m)\Gamma\bar{N}_{p,m}. \qquad (26)\end{aligned}$$

The total photon number fluctuation spectrum $\langle \Delta N_p^2(\omega)\rangle$, due to multilongitudinal amplified spontaneous emission, is given by [18]

$$\langle \Delta N_p^2(\omega)\rangle = \mathrm{Re}\left\{\sum_k\sum_l\langle \Delta N_{p,k}(\omega)\cdot\Delta N^*_{p,l}(\omega)\rangle\right\}. \qquad (27)$$

The normalized noise power spectrum $\langle i_n^2(\omega)\rangle$, detected by a photodetector with unity load resistance and unity bandwidth, is expressed by

$$\langle i_n^2(\omega)\rangle = \langle \Delta N_p^2(\omega)\rangle \times \frac{e^2}{\tau_{p2}^2}. \qquad (28)$$

Here, e is the electron charge, and $\tau_{p2}=[(C_0/L)\cdot\ln(1/\sqrt{R_2})]^{-1}$ is the photon lifetime determined by the output mirror reflectivity. The actual noise power $P_n(\omega)$ measured in an experiment is given by

$$P_n(\omega) = \langle i_n^2(\omega)\rangle\cdot R_L B_0 \eta_D^2. \qquad (29)$$

Here, η_D is the photodetector quantum efficiency including the coupling loss between a laser diode and a photodetector, B_0 is the detection bandwidth, and R_L is load resistance.

B. Photon Statistic Master Equation

Shimoda, Takahashi, and Townes (abbreviated as STT) have analyzed the noise characteristics of a traveling wave-type maser amplifier by means of a photon statistics master equation [14]. The rth order momentum of a photon number $\langle n^r\rangle$ is expressed by

$$\begin{aligned}\frac{d\langle n\rangle}{dt} &= \left(E_{cv,m}-E_{vc,m}-\frac{1}{\tau_p}\right)\langle n\rangle+E_{cv,m}, \qquad (30)\\ \frac{d\langle n^2\rangle}{dt} &= 2\left(E_{cv,m}-E_{vc,m}-\frac{1}{\tau_p}\right)\langle n^2\rangle\\ &+\left(3E_{cv,m}+E_{vc,m}+\frac{1}{\tau_p}\right)\langle n\rangle+E_{cv,m}, \qquad (31)\end{aligned}$$

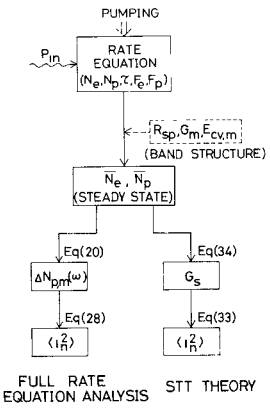

Fig. 1. Framework of the theoretical formulations.

$$\frac{d\langle n^r\rangle}{dt} = \sum_{j=0}^{r-1} \binom{\gamma}{j} \left[\langle (n+1) n^j \rangle E_{cv,m} + (-1)^{r+j} \langle n^{j+1} \rangle E_{vc,m} + (-1)^{r+j} \langle n^{j+1} \rangle \frac{1}{\tau_p} \right]. \tag{32}$$

This formulation has been extended to FP cavity type laser amplifiers, taking account of the input signal term and the FP resonant profile for multilongitudinal spontaneous emission photons [1]. The single-pass gain G_s is assumed to be constant over a single longitudinal mode.

Low-frequency noise power in the output of an FP cavity type amplifier is expressed by

$$\begin{aligned}\langle i_n^2 \rangle = e^2 \Bigg\{ & \frac{(1-R_1)(1-R_2)G_s}{(1-\sqrt{R_1R_2}\,G_s)^2} \langle n_0 \rangle \\ & + \sum_{m_l} \frac{(1+R_1G_s)(1-R_2)(G_s-1)\gamma m_t}{1-R_1R_2G_s^2} \left(\frac{C_0}{2L}\right) \\ & + 2\frac{(1+R_1G_s)(1-R_1)(1-R_2)^2 G_s(G_s-1)\gamma}{(1-\sqrt{R_1R_2}\,G_s)^4} \langle n_0 \rangle \\ & + \sum_{m_l} \frac{(1+R_1G_s)^2(1-R_2)^2(G_s-1)^2\gamma^2(1+R_1R_2G_s^2)m_t}{(1-R_1R_2G_s^2)^3} \\ & \cdot \left(\frac{C_0}{2L}\right) + \left[\frac{(1-R_1)(1-R_2)G_s}{(1-\sqrt{R_1R_2}\,G_s)^2}\right]^2 \\ & \cdot (\langle n_0^2 \rangle - \langle n_0 \rangle^2 - \langle n_0 \rangle) \Bigg\}. \end{aligned} \tag{33}$$

Here, $\langle n_0 \rangle$ is the mean photon number per second incident on the amplifier, R_1 and R_2 are, respectively, input and output mirror reflectivities, m_t is the number of transverse modes, C_0 is the light velocity in the amplifier medium, L is the amplifier length, and γ is the ratio of the spontaneous emission probability to the net gain coefficient $\gamma = E_{cv,m}/(E_{cv,m} - E_{vc,m})$.

The five terms on the right-hand side of (33) represent amplified shot noise, spontaneous emission shot noise, beat noise between signal and spontaneous emission, beat noise between spontaneous emission components, and signal excess noise. The last term disappears when the input signal is completely coherent.

Photon statistic master equation analysis (33) gives noise power as an analytic function of single-pass gain. Single-pass gain G_s should be calculated with the gain saturation effect, and is obtained by rate equation analysis. As shown in Fig. 1, the single-pass gain is expressed as

$$G_s = \exp\left[\left(\frac{1}{C_0} G_m \Gamma - \alpha_L\right) L\right] \tag{34}$$

where G_m [s^{-1}] is the stimulated emission coefficient given by (6), and α_L is the loss coefficient.

III. Comparison of Experimental and Theoretical Results

A. Experimental Procedure

A diagram of the experimental setup for the measurement of noise power and signal gain is shown in Fig. 2. The laser amplifier is a double-heterostructure AlGaAs laser of the transverse junction stripe type [21]. The emission wavelength is 840 nm and the cavity length is 200 μm. The oscillator was separated from the amplifier by an optical isolator with a 1 dB insertion loss and 32 dB isolation loss [22]. The oscillator and amplifier were mounted on copper heat sinks, which were temperature-controlled to within ±0.02°C.

Optical frequency matching and detuning between the input signal and amplifier FP longitudinal mode were achieved by varying the amplifier temperature and shifting the FP longitudinal mode frequency with respect to a stabilized oscillator frequency. Optical frequency tuning was observed by a television camera located at the exit slit of a monochromator.

Noise power was measured by a single detector technique [8]. The frequency response of the Si-APD and of following electronic amplifier circuits used for noise measurements, was calibrated by the white spectrum shot noise induced by irradiating an AlGaAs LED light.

Noise power $P_m(\omega)$ measured by the spectrum analyzer is expressed by

$$\begin{aligned} P_m(\omega) = & \{\eta_D^2 \langle i_n^2 \rangle_{\text{beat}} \langle g \rangle^2 + 2e\eta_D \langle i_{ph0} \rangle \langle g \rangle^{2+x}\} R_L B_0 G_e(\omega) \\ & + P_{\text{thermal}}(\omega) + P_{\text{dark current}}(\omega). \end{aligned} \tag{35}$$

Here, $\langle g \rangle$ is the avalanche multiplication factor of the Si-APD, $\langle i_{ph0} \rangle$ is the detector photocurrent when the total output power from the laser amplifier is detected with an APD having unity quantum efficiency and $\langle g \rangle = 1$, η_D is the product of the quantum efficiency of the Si-APD and the coupling efficiency

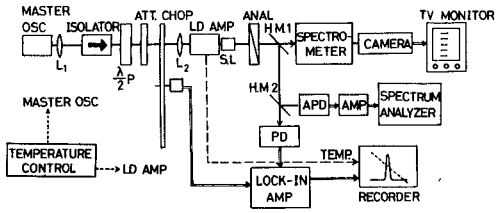

Fig. 2. Experimental setup for measuring noise power and signal gain with an AlGaAs laser amplifier. Amplifier is a TJS laser with 840 nm emission wavelength and 200 μm cavity length.

of the laser light output into the detector surface, B_0 is the resolution frequency bandwidth of a spectrum analyzer, R_L is the load resistance, $G_e(\omega)$ is the overall frequency response of the APD and electronic amplifier circuit, and $P_{\text{thermal}}(\omega)$ and $P_{\text{dark current}}(\omega)$ are the thermal noise power for measurement equipment and the APD dark current shot noise, respectively.

The first and the second terms on the right-hand side of (35) are the excess beat noise power and the conventional shot noise power, respectively. The shot noise power increases with APD gain by $\langle g\rangle^{2+x}$, where excess noise exponent x is 0.5 for the Si-APD [23]. On the other hand, the excess beat noise power increases with APD gain by $\langle g\rangle^2$, as shown in Fig. 3.

The relative noise power $\langle i_n^2\rangle$ of the laser amplifier output, which is defined in the previous section as the noise power generated in a unit of load resistance per unit of bandwidth in A^2/Hz, is expressed by

$$\langle i_n^2\rangle = \langle i_n^2\rangle_{\text{beat}} + 2e\langle i_{ph0}\rangle. \tag{36}$$

Excess beat noise power $\langle i_n^2\rangle_{\text{beat}}$ is calculated from (35) as

$$\langle i_n^2\rangle_{\text{beat}} = \frac{P_m(\omega) - P_{\text{thermal}}(\omega) - P_{\text{dark current}}(\omega)}{R_L B_0 G_e(\omega)\eta_D^2\langle g\rangle^2} - \frac{2e\langle i_{ph0}\rangle\langle g\rangle^x}{\eta_D}. \tag{37}$$

Relative noise power $\langle i_n^2\rangle$ is obtained from (36) and (37). The measured APD photocurrent $\langle i_{ph}^T\rangle$ in the avalanche multiplication condition is expressed by

$$\langle i_{ph}^T\rangle = \eta_D\langle i_{ph0}\rangle\langle g\rangle. \tag{38}$$

Noise power measurement was carried out under conditions where the avalanche multiplication factor $\langle g\rangle$ is 10 and the resolution bandwidth B_0 is 3 MHz. The coupling efficiency of the laser light output into the detector surface was - 9.0 dB measured with, and - 4.5 dB measured without optical signal injection. The quantum efficiency of the Si-APD was 0.7 at 840 nm.

Signal gain measurement was carried out by chopping the input beam at 200 Hz, and by using phase sensitive detection with a lock-in amplifier to eliminate the effect of spontaneous emission. By measuring the ratio v of the output signal power at a resonant condition to that at a nonresonant condition, the single-pass gain G_s and the overall signal gain G_{FP}, can be obtained as [4]

$$G_s = \frac{1}{\sqrt{R_1R_2}}\cdot\frac{\sqrt{v}-1}{\sqrt{v}+1}, \tag{39}$$

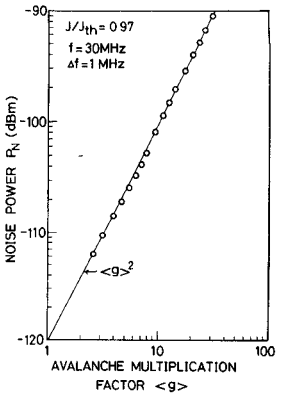

Fig. 3. Excess beat noise power detected by Si-APD versus avalanche multiplication factor. Laser is biased at $J/J_{\text{th}} = 0.97$, where beat noise power predominates over shot noise power. The light beam, chopped at a frequency of 225 Hz, is focused onto photosensitive area of Si-APD. Induced excess beat noise power is amplified by 30 MHz RF amplifier with 1 MHz bandwidth and is detected by calibrated lock-in amplifier [24].

$$G_{\text{FP}} = \left\{\frac{(1-\sqrt{R_1R_2}\,G_s)^2}{(1-R_1)(1-R_2)G_s} + \frac{4\sqrt{R_1R_2}}{(1-R_1)(1-R_2)}\cdot\sin^2\left[\frac{2\pi(\nu-\nu_0)L}{C_0}\right]\right\}^{-1}. \tag{40}$$

Here, ν is the incident signal optical frequency and ν_0 is the cavity resonant mode frequency. The modal facet mirror reflectivity R and the mode confinement factor Γ of this sample are, respectively, calculated to be 38 percent and 0.52, using a slab waveguide model [25].

The threshold was determined by intersection of the interpolation of the spontaneous emission and the stimulated emission power in the light output versus current characteristics. The threshold current of the amplifier was determined at the resonant condition temperature by taking account of the measured temperature dependence of the threshold current.

B. Total Noise Power in an AlGaAs Laser Amplifier

Experimental results on relative noise power $\langle i_n^2\rangle$, under signal injection, versus amplified signal level are shown in Fig. 4. The amplifier is biased at $J/J_{\text{th}} = 0.97$, where signal gain is measured to be 20 dB. The total noise power consists of amplified signal shot noise, spontaneous emission shot noise, beat noise between signal and spontaneous emission, and beat noise between spontaneous emission components. This is shown in Fig. 4.

Beat noise power between signal and spontaneous emission is obtained by subtracting the beat noise power between spontaneous emission components, which is measured without signal injection, from the total noise power which is measured at various injection signal levels. The shot noise powers are obtained by employing the same procedure as was mentioned above, in which the second term on the right-hand side of (36) is calculated using the measured detector photocurrent.

Beat noise powers predominate over the shot noise powers. The dominant noise in the laser amplifier is the beat noise between spontaneous emission components below the - 40 dBm input signal level. On the other hand, beat noise between signal

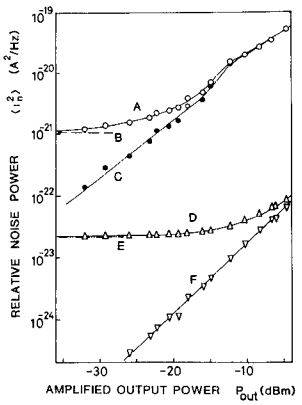

Fig. 4. Relative noise power at 500 MHz for AlGaAs laser amplifier is shown versus amplified signal level under signal injection. Relative noise power is defined as noise power generated with 1 Ω load resistance per unit bandwidth. Amplifier is biased at $J/J_{th} = 0.97$, where signal gain is measured to be 20 dB. J_{th} is the oscillation threshold current for the amplifier. A: Total noise, B: Beat noise between spontaneous emission components, C: Beat noise between signal and spontaneous emission, D: Total shot noise, E: Spontaneous emission shot noise, F: Signal shot noise.

and spontaneous emission is dominant above the −40 dBm input signal level.

Measured total noise power and theoretical values calculated by both rate equation analysis and photon statistic master equation analysis are shown in Fig. 5. They are given as functions of amplified signal output power. The experimental results are in reasonable agreement with both theoretical predictions.

The total noise power, calculated by the photon statistic master equation, can be broken down into two beat noise components. The beat noise power between spontaneous emission components begins to decrease at an amplified signal level higher than −10 dBm, due to the gain saturation effect. The beat noise power between signal and spontaneous emission increases with the amplified signal level. Its saturation at a high amplified signal level is not so strong as that in the beat noise power between spontaneous emission components.

C. Beat Noise Between Signal and Spontaneous Emission

Beat noise power between signal and spontaneous emission is shown in Fig. 6 as a function of the amplified signal level. Theoretical values derived by rate equation analysis are obtained by subtracting the beat noise power between spontaneous emission components, under no signal injection, from the total noise power at various injected signal levels. In the rate equation analysis the parameters are assumed to be: full bandwidth $2\Delta E$ for a positive net gain ($G_m > 0$) at 140 Å, loss coefficient α_L at 15 cm^{-1}, recombination coefficient B at 1×10^{-10} cm^3/s, and the band-tailing parameter E_0 at 20 meV.

The amplifier is biased at $J/J_{th} = 0.97$, where signal gain is 20 dB. Experimental results lie between curves calculated by rate equation analysis and photon statistic master equation analysis. Below −10 dBm, that is, the saturation output power [4] at which signal gain decreases by 3 dB from the unsaturated value, beat noise power between signal and spontaneous emission is proportional to amplified signal level $P_{out}[W]$, and is expressed by $\langle i_n^2 \rangle_{sig\text{-}sp} = 2 \times 10^{-16} \cdot P_{out}[W]$.

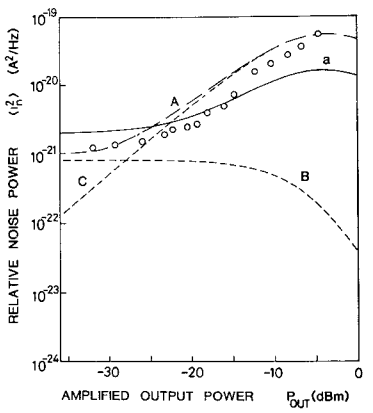

Fig. 5. Relative noise power versus amplified signal output. Experimental results are total noise power at 500 MHz. Solid line (a) is total noise power at 500 MHz calculated by rate equation analysis. Dash-dotted line (A) is total noise power calculated by photon statistic master equation analysis. Broken lines (B) and (C) are beat noise power between spontaneous emission components and between signal and spontaneous emission, respectively. They are calculated using photon statistic master equations. In numerical calculation, the parameters are assumed as follows: full bandwidth for a positive net gain is 140 Å, loss coefficient α_L is 15 cm^{-1}, recombination coefficient B is 1×10^{-10} cm^3/s, and band-tailing parameter E_0 is 20 meV.

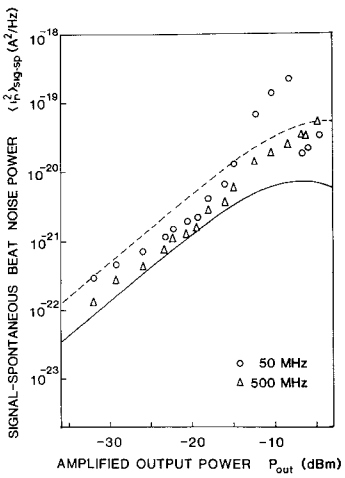

Fig. 6. Relative beat noise power between signal and spontaneous emission, versus amplified signal output power. Amplifier is biased at $J/J_{th} = 0.97$, where signal gain is 20 dB. Solid and broken lines are calculated low-frequency values obtained by rate equation analysis and photon statistic master equation analysis, respectively.

The beat noise power spectrum between signal and spontaneous emission at $J/J_{th} = 0.97$ is shown for various amplified signal levels in Fig. 7. Values calculated by the rate equations indicate that the noise spectrum is flat up to nearly 1 GHz and decreases with f^{-2} above 1 GHz for the low amplified signal level. However, for the high amplified signal level $P_{out} > -10$ dBm, resonance-like spectra appear. These seem to stem from the reduction of the threshold current by signal injection. The noise bandwidth for the low amplified signal level, at which the noise power decreases by 3 dB from the low-frequency value, coincides with the half width-half maximum gain bandwidth $\Delta\nu_{1/2}$ [4], which is expressed by

$$\Delta\nu_{1/2} = \frac{C_0}{2\pi L} \cdot \sin^{-1}\left\{\frac{\sqrt{(1-R_1)(1-R_2)}}{2(R_1R_2)^{1/4}} \cdot G_{FP}^{-1/2}\right\}. \quad (41)$$

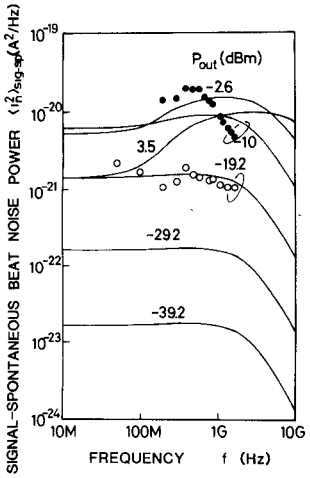

Fig. 7. Beat noise power spectra between signal and spontaneous emission. Signal gain of the amplifier is 20 dB. Solid lines are calculated by rate equation analysis.

D. Beat Noise Between Spontaneous Emission Components

Noise power without signal injection is shown in Fig. 8 as a function of dc bias current J/J_{th}. Theoretical values for various frequency components are calculated using the rate equations. Spontaneous emission shot noise power that is calculated from the measured detector photocurrent is also displayed by a dashed line.

Noise power in completely incoherent or coherent light is obtained except near the threshold and coincides with the shot noise level. Near the threshold, the beat noise between spontaneous emission components predominates over the shot noise by three or four orders of magnitude. Beat noise power between spontaneous emission components increases steeply when the pumping rate is above $J/J_{th} = 0.9$. Above the threshold, the higher the frequency component, the larger the maximum noise level attained at a high pumping rate. This reflects the resonance peak in the noise spectrum [9].

Beat noise power between spontaneous emission components just below the oscillation threshold, which is the operating region of the laser amplifier, is shown in Fig. 9 as a function of the pumping rate $1 - J/J_{th}$. Experimental results measured without signal injection lie between two theoretical values, that is, calculated by rate equation analysis and photon statistic master equation analysis. Beat noise power is independent of frequency up to 1500 MHz and increases with the pumping rate by $(1 - J/J_{th})^{-2.5}$.

Spectrum for the beat noise power between spontaneous emission components is shown for various pumping rates in Fig. 10. Values calculated by rate equation analysis indicate that below the oscillation threshold, the beat noise spectrum between spontaneous emission components is flat up to nearly 1 GHz, and decreases with f^{-2} above 1 GHz. Above the threshold, a resonance peak appears in the frequency range of from several hundred MHz to several GHz [9].

Beat noise power between spontaneous emission components is shown in Fig. 11 versus the signal gain. Signal gain is measured by the signal injection method [4] for various pumping rates, using (39) and (40). Experimental results on the beat noise power at the corresponding pumping rate are the same as shown in Fig. 9. They are plotted in Fig. 11.

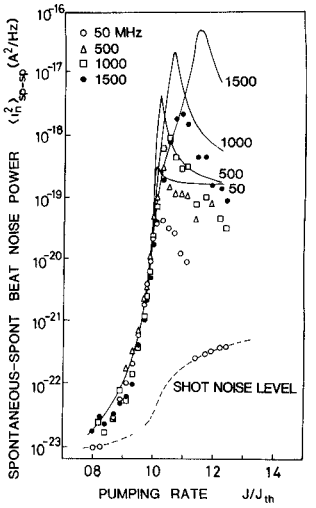

Fig. 8. Relative beat noise power between spontaneous emission components versus the amplifier pumping rate J/J_{th}, which is measured without input signal. Solid lines are calculated using the rate equations.

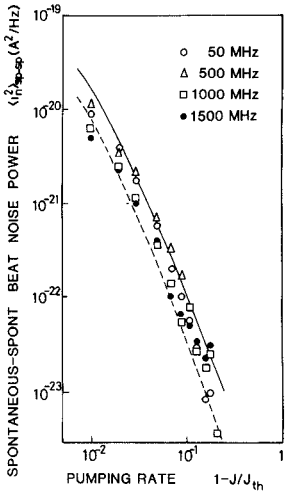

Fig. 9. Relative beat noise power between spontaneous emission components below the oscillation threshold versus the amplifier pumping rate $1 - J/J_{th}$. Solid and broken lines are calculated using the rate equations and photon statistic master equations, respectively.

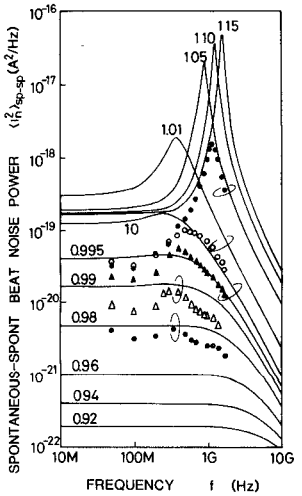

Fig. 10. Beat noise power spectra between spontaneous emission components. Calculated values are obtained by rate equation analysis.

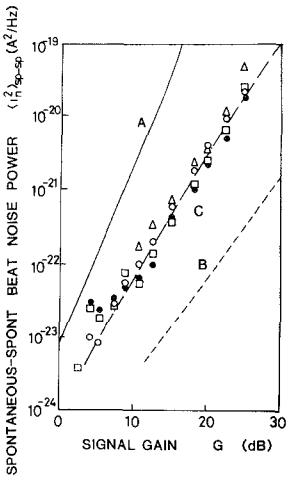

Fig. 11. Relative beat noise power between spontaneous emission components versus signal gain at a resonant condition. Solid line (A) is calculated by rate equation analysis. Broken line (B) is obtained from both the noise power calculated by photon statistic master equation analysis, and signal gain G_{FP}, calculated by active FP formulation. Dash-dotted line (C) is obtained from both the noise power calculated by rate equation analysis and the averaged gain G, which is given by the square-root product of G_{FP} and G_c. Here, G_c is the signal gain calculated by the rate equations.

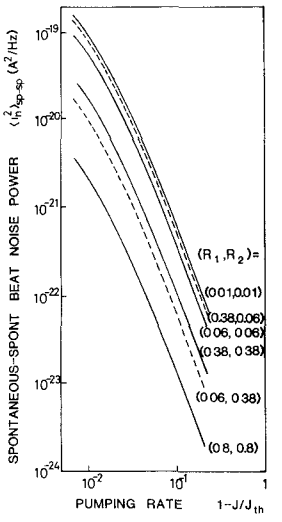

Fig. 12. Relative noise power between spontaneous emission components calculated by rate equation analysis versus the amplifier pumping rate $1 - J/J_{th}$. Solid and broken lines show the symmetrical and asymmetrical facet mirror reflectivity configurations, respectively. R_1 and R_2 are the input and output mirror reflectivities, respectively.

Theoretical curve A is calculated by rate equation analysis in which signal gain G_c is defined by (16) in [4] as the ratio of the increment of the photon number extracted from the output mirror to the injected photon number from outside the input mirror. Theoretical curve B is obtained from both the beat noise power calculated by photon statistic master equation analysis and the signal gain G_{FP} calculated by the active FP cavity formulation given by (40). The difference between these two theoretical curves stems from the underestimated signal gain in the rate equation analysis and the overestimated signal gain in the active FP formulation [4]. We have tentatively redefined signal gain G using the square-root product of G_c and G_{FP} ($=\sqrt{G_c G_{FP}}$). Calculated curve C that uses averaged signal gain G is in good agreement with experimental results. Beat noise power between spontaneous emission components increases with the signal gain by

$$\langle i_n^2 \rangle_{sp\text{-}sp} = 1.2 \times 10^{-24} \cdot G^{1.64}.$$

IV. Discussion

A. Improvement of Noise Characteristics

Beat noise between signal and spontaneous emission is inevitable in a laser amplifier. Beat noise between spontaneous emission components is, however, spurious and can be reduced.

Fig. 12 shows beat noise power between spontaneous emission components versus the pumping rate $1 - J/J_{th}$ for various facet mirror reflectivities. They are calculated by rate equation analysis.

Beat noise power at the same pumping rate is reduced by increasing the mirror reflectivities. This is due to the high-frequency selectivity of the FP cavity and reduced carrier density at the threshold. In an asymmetrical cavity structure, beat noise power in a configuration with high-input mirror reflectivity and low-output mirror reflectivity is larger than that in a configuration with low-input and high-output mirror reflectivities. The difference between these two configurations arises from the fact that the most spontaneous emission photons in the cavity are extracted from the low-reflectivity side.

Fig. 13 presents beat noise power between spontaneous emission components versus signal gain for various facet mirror reflectivities. Noise power is calculated by rate equation analysis, and signal gain G is tentatively defined by $\sqrt{G_c G_{FP}}$.

Reduction in mirror reflectivities gives rise to higher signal gain, due to improvement of the input and output coupling efficiency [4]. The degree of signal gain improvement exceeds degradation of noise characteristics resulting from reduction in mirror reflectivities. Comparing noise power under conditions where the same signal gain is obtained for various facet mirror reflectivities, reduction of mirror reflectivity gives rise to lower beat noise power between spontaneous emission components.

In an asymmetrical mirror reflectivity structure, nearly the same signal gain is available at the same dc bias level. Therefore, beat noise power between spontaneous emission components is reduced by the configuration providing low-input and high-output mirror reflectivities. Beat noise power between signal and spontaneous emission is also reduced by these configurations.

B. Equivalent Noise Bandwidth and Excess Noise Coefficient for an FP Cavity Type Laser Amplifier

Beat noise power between spontaneous emission components can be analytically expressed as a function of signal gain G by introducing the equivalent noise bandwidth Δf_{eq} in the manner

$$\langle i_n^2 \rangle_{sp\text{-}sp} = e^2 G^2 \Delta f_{eq}. \tag{42}$$

Here, e^2G^2 is the noise power per unit of optical gain bandwidth generated in an ideal traveling wave amplifier [14]. Equivalent noise bandwidth Δf_{eq} includes transverse and longi-

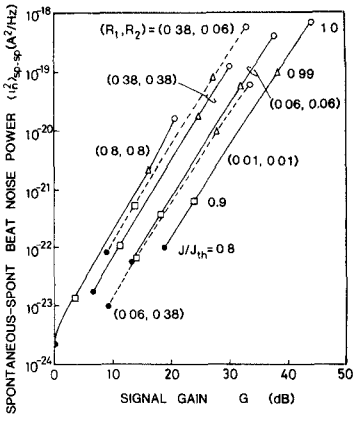

Fig. 13. Relative beat noise power between spontaneous emission components versus signal gain at a resonant condition. The noise power is calculated by rate equation analysis, and signal gain G is tentatively defined as the square-root product $\sqrt{G_c G_{FP}}$. Marks in the figure indicate pumping rate of 0.8, 0.9, 0.99, and 1.0, respectively.

tudinal multimode effects, as well as a factor of 2 for polarization modes.

The values of Δf_{eq}, derived from the theoretical noise power $\langle i_n^2 \rangle_{sp\text{-}sp}$ shown in Fig. 13, are tabulated in Table I. A narrower equivalent noise bandwidth is obtained by reducing the mirror reflectivity. This suggests that internal signal gain in a low Q cavity is lower than that in a high Q cavity at the same net signal gain G, and that the amount of noise power generated in the amplifying medium is smaller in the former case.

The dependence of equivalent noise bandwidth on signal gain stems from the gain bandwidth narrowing in (41) that is accompanied by the increase in the dc bias current by $G^{-0.5}$. Noise reduction effect due to the frequency selectivity of the FP cavity gives rise to a smaller equivalent noise bandwidth than that for a traveling wave type amplifier without a noise filter.

Beat noise power between signal and spontaneous emission can also be expressed analytically by introducing the excess noise coefficient χ in the manner

$$\langle i_n^2 \rangle_{sig\text{-}sp} = 2G(e^2/h\nu) P_{out} \chi. \tag{43}$$

Here, h is the Planck's constant, ν is the optical frequency, and P_{out} is the amplified signal level.

The values of χ calculated by photon statistic master equation analysis are also tabulated in Table I. The values of χ calculated by rate equation analysis are slightly lower than those calculated by photon statistic master equation analysis. The dependence of excess noise coefficient on signal gain stems from an internal signal gain in the FP cavity that is higher than that for a traveling wave amplifier. The excess noise coefficient χ decreases with reductions in mirror reflectivity and approaches $\chi = 1$, which is the value for an ideal traveling wave amplifier.

V. Conclusion

Noise characteristics for an FP cavity type laser amplifier were studied theoretically and experimentally. Quantum mechanical rate equations containing a Langevin shot noise source and an input signal term were solved for an exponential band-tail model with no k-selection rule. The photon statistic master equation method was also used to calculate the noise power. Experimental results on noise power for an AlGaAs laser amplifier were in reasonable agreement with both theoretical predictions. Noise behavior of the AlGaAs laser has been clarified by this work, in conjunction with Jäckel's [10], [18], for the pumping range below and above the threshold.

Noise characteristics for the FP cavity type semiconductor laser amplifier can be improved by both reducing the facet mirror reflectivities and using an asymmetric cavity configuration with low-input and high-output mirror reflectivities. The latter seems to have the advantage in the premature stage of the antireflection coating technique.

Equivalent noise bandwidth and excess noise coefficient are defined as the figures of merit of the FP cavity type optical amplifier. Two beat noise powers are expressed in simple analytic form by using these new parameters. The noise power characteristics against the amplified signal level, clarified here, enable us to calculate the signal-to-noise ratio S/N, and error rate performance of the laser amplifier system. Noise characteristics improve as the FP type amplifier approaches the traveling wave type amplifier.

Semiconductor laser amplifiers can be utilized in the future as preamplifiers, linear repeaters, and booster amplifiers both in a PCM-IM direct detection optical transmission system and a coherent optical fiber transmission system. The preamplifier, located in front of the photodetector so as to improve the minimum detectable power, is a promising candidate in wavelength regions above 1 μm, where the APD dark current becomes marked and available gain is limited to a low value. Linear amplifier repeaters between electronically regenerating terminal repeaters enlarge the regenerative repeater spacing by compensating for the attenuation due to fiber loss. This opens a possibility of transoceanic fiber cable systems without electronically regenerative repeaters. The booster amplifier, utilized to compensate for the insertion loss and power splitting loss in optical switches and power dividers, will be a key device in constructing optical subscriber loops. The performance of these optical direct amplification systems can be evaluated by the error rate characteristics, using the above-mentioned signal-to-noise ratio.

TABLE I
FIGURES OF MERIT OF FABRY-PEROT CAVITY TYPE OPTICAL AMPLIFIERS

Facet reflectivity [R_1 , R_2] L = 200 μm		Equivalent noise bandwidth * Δf_{eq} Gain dependence	Applicable range of gain (dB)	Value at G=20 dB	Excess noise coefficient ** χ Gain dependence	Applicable range of gain (dB)	Value at G=20 dB
Symmetric	[0.38, 0.38]	$6.1\times10^{13}\cdot G^{-0.38}$	7 - 30	1.1×10^{13}	$2.6\times G^{0.38}$	7 - 30	14.6
	[0.06, 0 06]	$1.7\times10^{13}\cdot G^{-0.38}$	13 - 36	2.7×10^{12}	$0.72\times G^{0.36}$	13 - 36	3.8
	[0.01, 0.01]	$4.4\times10^{12}\cdot G^{-0.45}$	9 - 40	5.6×10^{11}	$0.36\times G^{0.32}$	9 - 40	1.6
Asymmetric	[0.38, 0.06]	$1.2\times10^{14}\cdot G^{-0.37}$	9 - 33	2.1×10^{13}	$3.4\times G^{0.39}$	9 - 33	20
	[0.06, 0.38]	$1.25\times10^{13}\cdot G^{-0.38}$	9 - 33	2.1×10^{12}	$1.0\times G^{0.34}$	9 - 33	4.9
TW type	[0 , 0]	Independent of gain		3.2×10^{12} ***	Independent of gain		1

* $\Delta f_{eq} = \dfrac{\langle i_{n\ sp\text{-}sp}^2 \rangle}{e^2 G^2}$; see Eq.(42)

** $\chi = \dfrac{\langle i_{n\ sig\text{-}sp}^2 \rangle}{2\,G\,(e^2/h\nu)\,P_{out}}$; see Eq.(43)

*** Value calculated by photon statistic master equation using Eq (6) with ΔE = 70 Å.

ACKNOWLEDGMENT

The authors wish to thank Dr. T. Kimura and A. Kawana for useful suggestions and discussions.

REFERENCES

[1] Y. Yamamoto, "Noise and error rate performance of semiconductor laser amplifiers in PCM-IM optical transmission systems," *IEEE J. Quantum Electron.*, vol. QE-16, pp. 1073-1081, Oct. 1980.

[2] Y. Yamamoto and T. Kimura, "Coherent optical fiber transmission systems," *IEEE J. Quantum Electron.*, vol. QE-17, pp. 919-935, June 1981.

[3] S. Kobayashi and T. Kimura, "Gain and saturation power of resonant AlGaAs laser amplifier," *Electron. Lett.*, vol. 16, pp. 230-232, 1980.

[4] T. Mukai and Y. Yamamoto, "Gain, frequency bandwidth, and saturation output power of AlGaAs laser amplifiers," *IEEE J. Quantum Electron.*, vol. QE-17, pp. 1028-1034, June 1981.

[5] F. Favre, L. Jeunhomme, I. Joindt, M. Monerie, and J. C. Simon, "Progress toward heterodyne-type single-mode fiber communication systems," *IEEE J. Quantum Electron.*, vol. QE-17, pp. 897-906, June 1981.

[6] Y. Yamamoto and H. Tsuchiya, "Optical receiver sensitivity improvement by a semiconductor laser preamplifier," *Electron. Lett.*, vol. 16, pp. 233-235, 1980.

[7] Y. Yamamoto, "Characteristics of AlGaAs Fabry-Perot cavity type laser amplifiers," *IEEE J. Quantum Electron.*, vol. QE-16, pp. 1047-1052, Oct. 1980.

[8] J. Armstrong and A. W. Smith, "Intensity fluctuations in GaAs laser emission," *Phys. Rev.*, vol. 140, pp. A155-164, Oct. 1965.

[9] T. L. Paoli, "Noise characteristics of stripe-geometry D.H. junction laser operating continuously—I. Intensity noise at room temperature," *IEEE J. Quantum Electron.*, vol. QE-11, pp. 276-283, June 1975.

[10] H. Jäckel and H. Melchior, "Fundamental limit of the light intensity fluctuations of semiconductor lasers with dielectric transverse mode confinement," presented at Opt. Commun. Conf., Amsterdam, The Netherlands, Sept. 17-19, 1979.

[11] T. Mukai and Y. Yamamoto, "Noise characteristics of semiconductor laser amplifiers," *Electron. Lett.*, vol. 17, pp. 31-33, Jan. 1981.

[12] D. E. McCumber, "Intensity fluctuations in the output of CW laser oscillators. I," *Phys. Rev.*, vol. 141, pp. 306-322, Jan. 1966.

[13] M. J. Adams, "Theoretical effects of exponential bandtails on the properties of the injection laser," *Solid-State Electron.*, vol. 12, pp. 661-669, 1969.

[14] K. Shimoda, H. Takahashi, and C. H. Townes, "Fluctuations in amplification of quanta with application to master amplifiers," *J. Phys. Soc. Japan*, vol. 12, pp. 686-700, June 1957.

[15] H. Haug, "Quantum-mechanical rate equations for semiconductor lasers," *Phys. Rev.*, vol. 184, pp. 338-348, Aug. 1969.

[16] D. J. Morgan and M. J. Adams, "Quantum noise in semiconductor lasers," *Phys. Status Solidi (a)*, vol. 11, pp. 243-253, 1972.

[17] M. Lax, "Quantum noise VII: The rate equation and amplitude noise in lasers," *IEEE J. Quantum Electron.*, vol. QE-3, pp. 37-46, Feb. 1967.

[18] H. Jäckel, "Light intensity fluctuations and dynamic behavior of AlGaAs heterostructure diode lasers in the frequency range of 10 MHz to 8 GHz," Ph.D. dissertation, Tech. Univ. of Zürich, Zürich, Switzerland, 1980.

[19] H. Jäckel and G. Guekos, "High-frequency intensity noise spectra of axial mode groups in the radiation from CW GaAlAs diode lasers," *Opt. Quantum Electron.*, vol. 9, pp. 233-239, 1977.

[20] T. Ito, S. Machida, K. Nawata, and T. Ikegami, "Intensity fluctuations in each longitudinal mode of a multimode AlGaAs laser," *IEEE J. Quantum Electron.*, vol. QE-13, pp. 574-579, 1977.

[21] H. Namizaki, "Transverse-junction-stripe lasers with a GaAs p-n homojunction," *IEEE J. Quantum Electron.*, vol. QE-11, pp. 427-431, July, 1975.

[22] K. Kobayashi and M. Seki, "Microoptic grating multiplexers and optical isolators for fiber-optic communications," *IEEE J. Quantum Electron.*, vol. QE-16, pp. 11-22, Jan. 1980.

[23] H. Kanbe, T. Kimura, Y. Mizushima, and K. Kajiyama, "Silicon avalanche photodiodes with low multiplication noise and high-speed response," *IEEE Trans. Electron Devices*, vol. ED-23, pp. 1337-1343, Dec. 1976.

[24] O. Mikami, H. Ando, H. Kanbe, T. Mikawa, T. Kaneda, and Y. Toyama, "Improved germanium avalanche photodiodes," *IEEE J. Quantum Electron.*, vol. QE-16, pp. 1002-1007, Sept. 1980.

[25] T. Ikegami, "Reflectivity of mode at a facet and oscillation mode in double-heterostructure injection lasers," *IEEE J. Quantum Electron.*, vol. QE-8, pp. 470-476, June 1972.

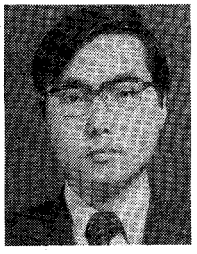

Takaaki Mukai was born in Osaka, Japan, on January 22, 1952. He received the B.S. and M.S. degrees in electronics engineering from Osaka University, Osaka, Japan, in 1975 and 1977, respectively.

In 1977 he joined the Musashino Electrical Communication Laboratory, Nippon Telegraph and Telephone Public Corporation, Tokyo, Japan. He has been engaged in research on the characteristics of semiconductor lasers and optical amplifiers.

Mr. Mukai is a member of the Institute of Electronics and Communication Engineers of Japan and the Japan Society of Applied Physics.

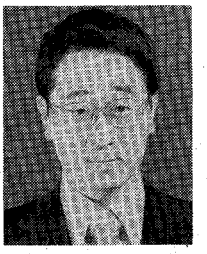

Yoshihisa Yamamoto (S'75-M'80) was born in Tokyo, Japan, on November 21, 1950. He received the B.S. degree from the Tokyo Institute of Technology, Tokyo, Japan, in 1973, and the S.M. and Ph.D. degrees from the University of Tokyo, Tokyo, Japan, in 1975 and 1978, respectively.

Since joining the Musashino Electrical Communication Laboratory, Nippon Telegraph and Telephone Public Corporation, Tokyo, Japan, in 1978, he has been engaged in research on photodetectors for optical communication, optical amplifiers, and coherent optical transmission systems.

Dr. Yamamoto is a member of the Institute of Electronics and Communication Engineers of Japan and the Japan Society of Applied Physics.

Optical FM Signal Amplification by Injection Locked and Resonant Type Semiconductor Laser Amplifiers

SOICHI KOBAYASHI, MEMBER, IEEE, AND TATSUYA KIMURA, SENIOR MEMBER, IEEE

Abstract—**Optical FM signal amplification by semiconductor lasers is studied by emphasizing their bandwidth characteristics. The laser is operated either in an injection-locked mode or in a resonant amplification mode by keeping the drive current above or just below its threshold.**

The bandwidths of both amplifiers are evaluated by the reduction in modulation sidebands and are compared with the bandwidths measured statically by scanning the frequency of incident CW wave. The $\sqrt{G}B$ = 25 GHz gain bandwidth product is obtained for both operation modes using a double heterostructure AlGaAs semiconductor laser.

The bandwidth obtained in the above procedure is in good agreement with theoretical results.

I. Introduction

COHERENT optical transmission systems, in which optical amplitude, frequency, or phase are modulated to carry information and are demodulated by heterodyne detection, are expected to improve optical fiber communication system performance, resulting in long repeater spacing and large information capacity [1]. The possibility of a coherent FM signal transmission system using a semiconductor laser transmitter and an independent local oscillator has successfully been demonstrated [2].

Important technologies related to a coherent FSK system have been studied using semiconductor lasers. Direct frequency modulation in a semiconductor laser has been studied theoretically and experimentally [3]. Semiconductor laser spectral line shape observation and linewidth reduction to less than 50 kHz, with an external grating feedback, have been reported [4]. Furthermore, single longitudinal mode operation of a semiconductor laser, directly modulated at a high data rate, has been realized by injection locking [5]. An injection-locked amplifier (ILA) and resonant type amplifier (RTA) performance using AlGaAs semiconductor lasers have also been studied for CW or AM modulated input [6], [7].

This paper reports on amplification of frequency modulated optical waves by semiconductor lasers operating in ILA and RTA modes. Evaluation of bandwidth characteristics for the two operation modes shows that the gain bandwidth product is given by $\sqrt{G}B$ = 25 GHz in a double heterostructure AlGaAs semiconductor laser. The bandwidth was measured by observing sideband amplitudes of frequency modulated waves at the input and output of the amplifier.

The above results on bandwidth are in good agreement with theoretical values. FM signal amplification was measured in microwave solid-state devices [8], [9]. Compared to these devices, the ILA operation of semiconductor lasers enables broad-band operation, since the carrier frequency is by far higher than that at microwaves. The ILA operation for a semiconductor laser, as well as the RTA operation, will be useful as devices for transmitters and receivers in future coherent optical transmission systems.

Manuscript received September 1, 1981; revised November 1, 1981.

The authors are with the Musashino Electrical Communication Laboratory, Nippon Telegraph and Telephone Public Corporation, Tokyo, Japan.

0018-9480/82/0400-0421$00.75